Article

Red Light in Chemiluminescence and Yellow-Green Light in Bioluminescence: Color-Tuning Mechanism of Firefly, *Photinus pyralis*, Studied by the Symmetry-Adapted Cluster–Configuration Interaction Method

Naoki Nakatani, Jun-ya Hasegawa, and Hiroshi Nakatsuji

J. Am. Chem. Soc., **2007**, 129 (28), 8756-8765• DOI: 10.1021/ja0611691 • Publication Date (Web): 22 June 2007

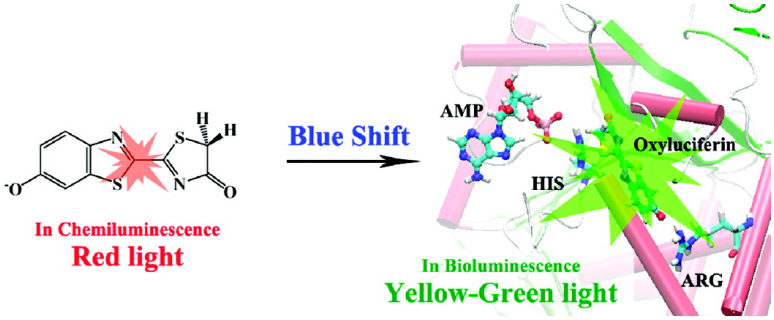

More About This Article

Additional resources and features associated with this article are available within the HTML version:

- Supporting Information
- Links to the 7 articles that cite this article, as of the time of this article download
- Access to high resolution figures
- Links to articles and content related to this article
- Copyright permission to reproduce figures and/or text from this article

View the Full Text HTML

J|A|C|S
ARTICLES
Published on Web 06/22/2007

Red Light in Chemiluminescence and Yellow-Green Light in Bioluminescence: Color-Tuning Mechanism of Firefly, *Photinus pyralis*, Studied by the Symmetry-Adapted Cluster−Configuration Interaction Method

Naoki Nakatani,[†] Jun-ya Hasegawa,[†,§] and Hiroshi Nakatsuji*[,†,§]

Contribution from the Department of Synthetic Chemistry and Biological Chemistry, Graduate School of Engineering, Kyoto University, Kyoto-Daigaku-Katsura, Nishikyo-ku, Kyoto 615-8510, Japan, and Quantum Chemistry Research Institute (QCRI), Kyodai Katsura Venture Plaza, Goryou Oohara 1-36, Nishikyo-Ku, Kyoto 615-8245, Japan

Received February 17, 2006; E-mail: h.nakatsuji@qcri.or.jp

Abstract: The yellow-green luminescence from firefly luciferase has long been understood to be the emission from enol-oxyluciferin. However, a recent experiment showed that an oxyluciferin constrained to the keto form produced a yellow-green emission in luciferase (Branchini, B. R.; Murtiashaw, M. H.; Magyar, R. A.; Portier, N. C.; Ruggiero, M. C.; Stroh, J. G. *J. Am. Chem. Soc.* **2002**, *124*, 2112-2113). The present quantum mechanical/molecular mechanical and symmetry-adapted cluster−configuration interaction (SAC−CI) theoretical study supports the keto-form to be the yellow-green bioluminescence state in luciferase. We give the theoretically optimized structure of the excited state of oxyluciferin within luciferase, which gives luminescence calculated by the SAC−CI method that is close to the experimental value. Coulombic interactions with neighboring residues, in particular Arg218 and the phosphate group of AMP, play important roles in the color-tuning mechanism. Transformation to the enol form is energetically unfavorable in the luciferase environment. The twisted intramolecular charge-transfer (TICT) state is meta stable and would be easily relaxed to the co-planer structure. Further analyses were performed to verify the spectral-tuning mechanism based on the protonation state and the resonance structure of oxyluciferin.

Introduction

Bioluminescence is a well-known photobiological phenomenon in which chemical energy is converted into photon energy. Firefly luminescence is a typical example of bioluminescence. There are about two thousand types of firefly worldwide, and the color of the emission varies from green (∼530 nm) to red (∼635 nm) depending on the species.[1] The enzyme firefly luciferase (Luc) is also used in molecular imaging as a reporter of gene expression.[2] Therefore, the underlying molecular mechanism of color tuning must be clarified.

The mechanism of firefly bioluminescence proposed in previous studies[3,4] is summarized in Figure 1a. Luc binds firefly luciferin ((*S*)-2-(6-hydroxy-2-benzothiazolyl)-2-thiazoline-4-carboxylic acid, D-LH_2) in its active site and catalyzes the formation of luciferyl adenosine monophosphate (AMP). Initiated by the attachment of O_2 to the thiazoline ring, a dioxyetanone intermediate is formed via intramolecular chemically initiated electron-exchange luminescence (CIEEL).[5] In the final step, detachment of CO_2 generates oxyluciferin ($OxyLH_2$) in an electronically excited state, which produces a yellow-green emission in the case of the North American firefly (*Photinus pyralis*).[3,6] $OxyLH_2$ also exhibits chemiluminescence, with a mechanism very similar to that of bioluminescence, as shown in Figure 1b. It has been established that $OxyLH_2$ is in the keto form in dimethyl sulfoxide (DMSO) solution containing a small amount of potassium *tert*-butoxide (K[*tert*-BuO]). It is transformed into the enol form in DMSO solution with a large amount of K[*tert*-BuO].[6−8] The keto and enol isomers emit red (∼620 nm, 1.97 eV) and green (∼560 nm, 2.20 eV) light, respectively.[7] Because of the similarity between chemiluminescence and bioluminescence, the mechanism of color tuning in bioluminescence was believed to be the same as that in chemiluminescence.[6,7]

Recently, Branchini and co-workers[9] reported that 5,5-dimethyloxyluciferin that was constrained to exist only in the

[†] Kyoto University.
[§] Quantum Chemistry Research Institute (QCRI).

(1) (a) Wood, K. V. *Photochem. Photobiol.* **1995**, *62*, 662. (b) Wood, K. V.; Lam, Y. A.; Seliger, H. H.; McElroy, W. D. *Science* **1989**, *244*, 700. (c) Viviani, V. R; Bechara, E. J. H. *Photochem. Photobiol.* **1995**, *62*, 490. (d) Viviani, V. R. *Cell. Mol. Life Sci.* **2002**, *59*, 1833. (e) Ugarova, N. N. *Biolum. Chemilum.* **1989**, *4*, 406.
(2) Kricka, L. J. *Methods Enzymol.* **2000**, *305*, 333.
(3) Deluca, M. *Adv. Enzymol.* **1976**, *44*, 37.
(4) (a) Deluca, M.; Leonard, N. J.; Gates, B. J.; McElroy, W. D. *Proc. Natl. Acad. Sci. U.S.A.* **1973**, *70*, 1664. (b) DeLuca, M.; McElroy, W. D. *Biochemistry* **1974**, *13*, 921.
(5) McCapra, F. *J. Chem. Soc., Chem. Commun.* **1977**, 946. Koo, J.-Y.; Schmidt, S. P.; Schuster, G. B. *Proc. Natl. Acad. Sci. U.S.A.* **1978**, *75*, 30. Schuster, G. B. *Acc. Chem. Res.* **1979**, *12*, 366.
(6) White, E. H.; Rapaport, E.; Seliger, H. H.; Hopkins, T. A. *Bioorg. Chem.* **1971**, *92*.
(7) White, E. H.; Rapaport, E.; Hopkins, T. A.; Seliger, H. H. *J. Am. Chem. Soc.* **1969**, *91*, 2178.
(8) White, E. H.; Steinmetz, M. G.; Miano, J. D.; Wildes, P. D.; Morland, R. *J. Am. Chem. Soc.* **1980**, *102*, 3199.
(9) Branchini, B. R.; Murtiashaw, M. H.; Magrar, R. A.; Portier, N. C.; Ruggiero, M. C.; Stroh, J. G. *J. Am. Chem. Soc.* **2002**, *124*, 2112.

10.1021/ja0611691 CCC: $37.00

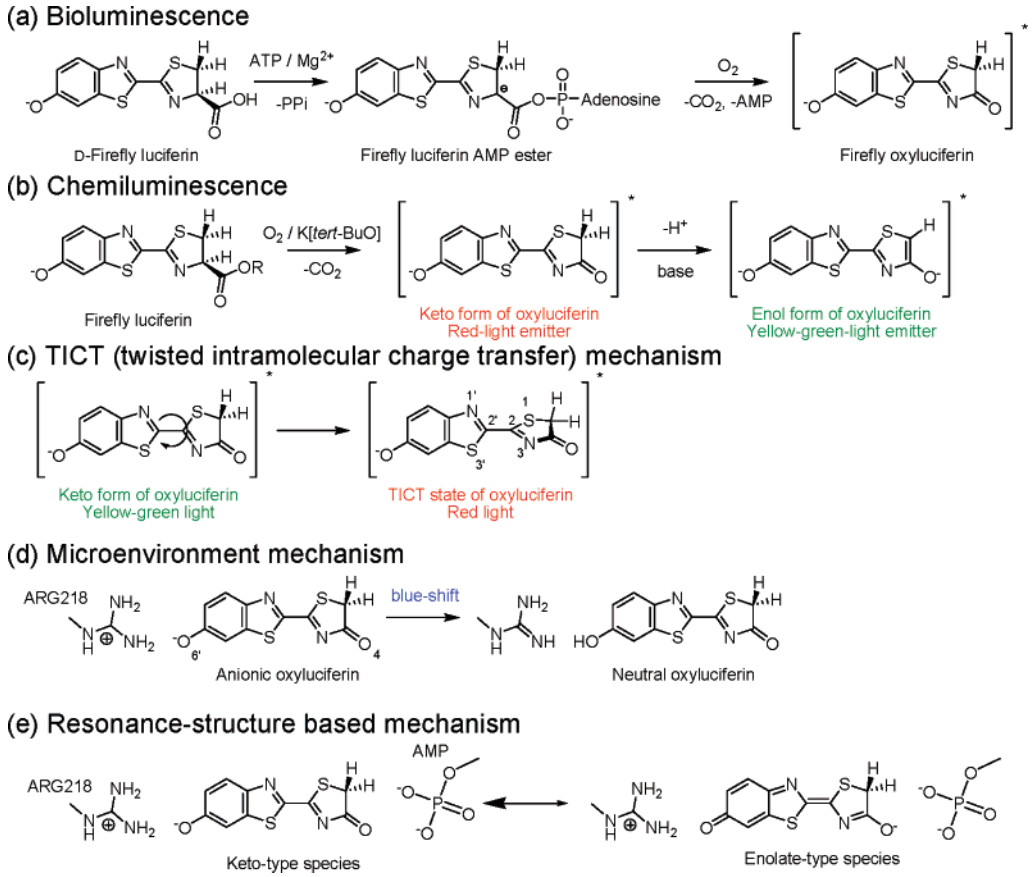

Figure 1. Proposed mechanism for (a) bioluminescence and (b) chemiluminescence of the firefly.[7] Other mechanisms for firefly bioluminescence: (c) TICT (twisted-intramolecular charge-transfer) mechanism,[11] (d) microenvironment mechanism,[12−14] and (e) resonance structure-based mechanism (see text for details).[10]

keto form produced green emission inside Luc.[9,10] This indicates that the color of the luminescence can be controlled only in the keto form. It is not necessary to invoke keto−enol tautomerism to explain the color of the bioluminescence.

At present, there are three alternative explanations. The first is the twisted intramolecular charge-transfer (TICT) state mechanism proposed by McCapra and co-workers and shown in Figure 1c.[11] Their semiempirical AM1 calculation suggests that twisting the C2−C2′ angle stabilizes the emitting state and produces the red emission. The planer structure that produces the yellow-green emission is a saddle point on the potential surface. The second explanation is the "microenvironment mechanism", which is shown schematically in Figure 1d.[12−14] In the keto form, the protonation state of the O6′ atom and Arg 218 (polarity of the hydrogen bond) is especially important.[14] The third proposal is related to the resonance structure of the excited $OxyLH_2$ in keto and enolate forms, as shown in Figure 1e.[10] The weights of the two resonance structures are equivalent in chemiluminescence, thereby stabilizing the emitting state. In the Luc environment, however, the local interaction constrains the resonance structure more to the left, which causes a blue-shift of the emission.[10] It is now necessary to characterize the electronic and molecular structures of the emitting state in the Luc environment and to clarify the mechanism of color tuning.

Since luminescence is a transient phenomenon during the photochemical process, reliable quantum mechanical (QM) calculations would provide useful information on the nature of the excited-state involved. Based on the X-ray structure[15] and working model provided by the previous experimental studies,[16,17] we performed molecular mechanical (MM) and QM calculations to determine the structure of the $OxyLH_2$-Luc binding complex in the excited state. For studying luminescence originating from molecular excited state, electron-correlation effects are essential for reproducing the excitation/emission energy in QM calculations. We used the symmetry-adapted cluster[1818]/symmetry-adapted cluster−configuration interaction (SAC/SAC−CI)[19] method[20] for balanced description of the electron correlation effects in both ground and excited states. One of the computationally inexpensive alternative approaches

(10) Branchini, B. R.; Southworth, T. L.; Murtiashaw, M. H.; Magyer, R. A.; Gonzalez, S. A.; Ruggiero, M. C.; Stroh, J. G. *Biochemistry* **2004**, *43*, 7255.
(11) McCapra, F.; Gilfoyle, D. J.; Young, D. W.; Church, N. J.; Spencer, P. *Bioluminescence and Chemiluminescence. Fundamentals and Applied Aspects*; Campbell, A. K., Kricka, L. J., Stanley, P. E. Eds.; John Wiley & Sons: Chichester, U.K., 1994; pp 387.
(12) DeLuca, M. *Biochemistry* **1969**, *8*, 160.
(13) (a) Ugarova, N. N.; Brovko, L. Y. *Luminescence* **2002**, *17*, 321. (b) Gandelman, O. A.; Brovko, L. Y.; Ugarova, N. N.; Chikishev, A. Y.; Shkurimov, A. P. *J. Photochem. Photobiol. B* **1993**, *19*, 187.
(14) Orlova, G.; Goddard, J. D.; Brovko, L. Y. *J. Am. Chem. Soc.* **2003**, *125*, 6962.
(15) Conti, E.; Franks, N. P.; Brick, P. *Structure* **1996**, *4*, 287.
(16) (a) Branchini, B. R.; Magyar, R. A.; Murtiashaw, M. H.; Anderson, S. M.; Zimmer, M. *Biochemistry* **1998**, *37*, 15311. (b) Branchini, B. R.; Magyar, R. A.; Murtiashaw, M. H.; Anderson, S. M.; Helgerson, L. C.; Zimmer, M. *Biochemistry* **1999**, *38*, 13223. (c) Branchini, B. R.; Southworth, T. L.; Murtiashaw, M. H.; Boije, H.; Fleet, S. E. *Biochemistry* **2003**, *42*, 10429.
(17) Branchini, B. R.; Magyar, R. A.; Murtiashaw, M. H.; Portier, N. C. *Biochemistry* **2001**, *40*, 2410.
(18) Nakatsuji, H.; Hirao, K. *J. Chem. Phys.* **1978**, *68*, 2053.
(19) (a) Nakatsuji, H. *Chem. Phys. Lett.* **1978**, *59*, 362. (b) Nakatsuji, H. *Chem. Phys. Lett.* **1989**, *67*, 329. (c) Nakatsuji, H. *Chem. Phys. Lett.* **1989**, *67*, 334.
(20) Nakatsuji, H. *Computational Chemistry, Reviews of Current Trends*; Leszczynski, J., Ed.; World Scientific: Singapore, 1996; Vol. 2, pp 62.

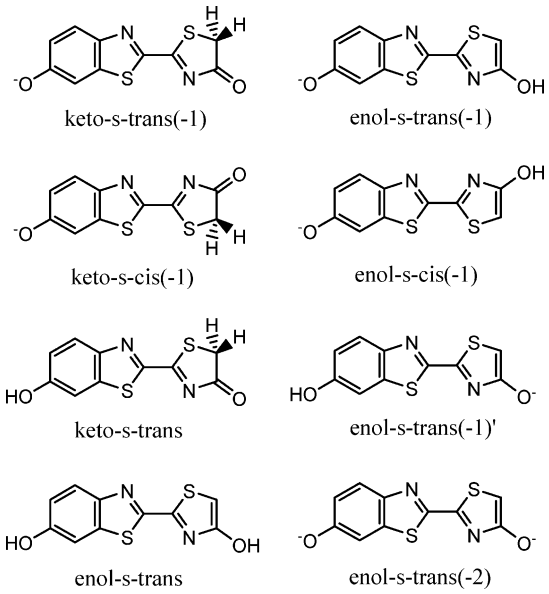

Figure 2. Structural isomers and tautomers of $OxyLH_2$ in different protonation states investigated in the present study.

may be the time-dependent density-functional theoretical (TD-DFT) calculation. However, the accuracy of the TDDFT is out of the required accuracy for photobiology, so that the TDDFT is useless for clarifying the underlying principle behind the photobiological phenomena. There are already several reports concerning the difficulties in the TDDFT method.[21] In our experience, TD-B3LYP calculations failed to systematically reproduce the excitation energies of retinal proteins.[21e] Since the excitation phenomena of $OxyLH_2$ in the Luc environment are such an unresolved problem, we did not perform TDDFT calculations to avoid introducing unnecessary confusions in the analyses.

In the present paper, we study with the SAC/SAC−CI method the chemiluminescence in DMSO solution and the bioluminescence in Luc. We will show that the keto form of $OxyLH_2$ produces red light in chemiluminescence and yellow-green in bioluminescence. We also examine the TICT state, the possibility of the enol form, and the effect of the local environmental on the protonation state - resonance structure of $OxyLH_2$.

Computational Details

Quantum Mechanical Calculations. In the study of chemiluminescence, we examined several structural isomers and tautomers of $OxyLH_2$ in different protonation states as shown in Figure 2. We adopted a conventional nomenclature[14] in which "keto" and "enol" indicate keto and enol (enolate) forms in the thiazol ring, respectively. The number in the parenthesis shows total charge of $OxyLH_2$. For enol-*s*-trans(-1)′, the prime indicates a protonation state different from that of enol-*s*-trans(-1). The geometries of their first excited states were optimized using the CI-single (CIS) method, and single-point SAC−CI calculations were performed at the optimized geometries for obtaining the fluorescence energies. Since the wave functions of the first excited states were well described by the one-electron transitions

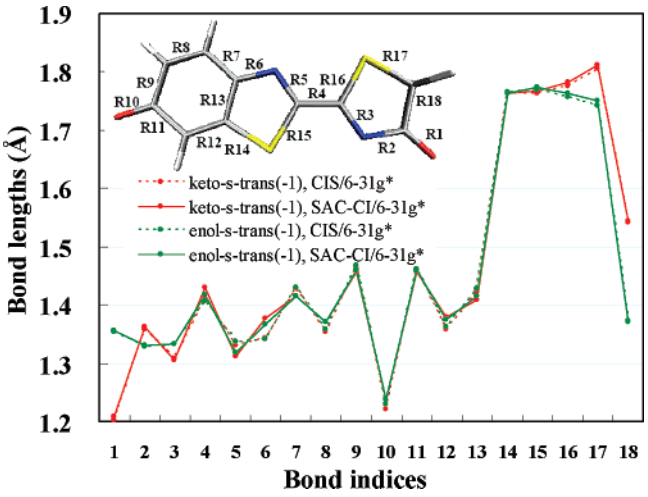

Figure 3. Bond lengths of keto and enol $OxyLH_2$ calculated by CIS and SAC−CI method in the gas phase.

from HOMOs to LUMOs, the CIS geometries were qualitatively correct. Actually, we performed also the SAC−CI geometry optimizations for the first excited states of keto-*s*-trans(-1) and enol-*s*-trans(-1) in a gas phase. In Figure 3 and Table S2 (Supporting Information), bond lengths obtained by CIS and SAC−CI methods are summarized. The rms deviation between the CIS and SAC−CI results was 0.014 and 0.010 Å in the keto and enol forms, respectively. The largest deviation is in the R6 (N−C) bond in both keto and enol forms, and the CIS bond length is about 0.03 Å shorter than the SAC−CI one. With the CIS and SAC−CI geometries, the calculated SAC−CI fluorescence energies of the keto form were 1.97 and 1.84 eV, respectively, and for the enol form, they were 2.04 and 2.01 eV, respectively. The correlation effect on the geometry of the excited-state was very small (0.03 eV) in the enol form, but it was not negligible in the keto form (0.13 eV = 3.07 kcal/mol). However, such differences were fortunately small enough not to affect the conclusions of the present paper. In the SAC−CI calculations, we performed perturbation selection for the double excitation operators[22] and the energy thresholds of 5.0×10^{-6} and 5.0×10^{-7} hartree (level two) were used for the ground and excited states, respectively. These calculations were performed in both the gas phase and DMSO solution. To mimic the DMSO environment, a polarized continuum model (PCM)[23] was used to take into account the solvation effects. The dielectric constant of DMSO ($\epsilon = 46.7$) was applied. The experimental solution also included K[*tert*-BuO]: 10^{-5} M LH_2 and 0.005−0.5 M K[*tert*-BuO] in DMSO solution.[6,7] To examine the effect of the coordination to the counterion, the K^+ ions were explicitly included in the QM models of the charged species: keto-*s*-trans(-1), enol-*s*-trans(-1), enol-*s*-trans(-1)', and enol-*s*-trans(-2). The geometry of the $OxyLH_2$-K^+ complex was also optimized using the CIS method with the PCM. For the basis sets, we used Huzinaga−Dunning double-ζ basis sets[24] augmented with the single-polarization d-function,[24] D95-(d), for the calculations of both geometries and fluorescence energies.

To evaluate the possibility of a TICT excited state, we studied the potential energy curve for twisting of the C2−C2′ bond (Figure 1c) in a gas phase. The geometry optimizations were done at the CIS/D95(d) level and the single-point SAC−CI calculations with D95(d) basis sets were done at the optimized geometries. The dihedral angle was rotated from 0.0° (trans) to 180.0° (cis) in steps of 10.0°. Since we used perturbation selection for the double excitation operators, we took the group sum of the excitation operators selected at each point of the

(21) (a) Casida, M. E.; Jamorski, C.; Casida, K. E.; Salahub, D. R. *J. Chem. Phys.* **1998**, *108*, 4439. Casida, M. E.; Salahub, D. R. *J. Chem. Phys.* **2000**, *113*, 8918. (b) Appel, F.; Gross, E. K. U.; Burke, K. *Phys. Rev. Lett.* **2003**, *90*, 043005. (c) Hsu, C.-P.; Hirata, S.; Head-Gordon, M. *J. Phys. Chem. A* **2001**, *105*, 451−458. (d) Dreuw, A.; Weisman, J. L.; Head-Gordon, M. *J. Chem. Phys.* **2003**, *119*, 2943−2946. (e) Milet, A.; Korona, T.; Moszynski, R.; Kochanski, E. *J. Chem. Phys.* **1999**, *111*, 7727. (f) Fujimoto, K.; Hayash, S.; Hasegawa, J.; Nakatsuji, H. *J. Chem. Theory Comput.* **2007**, *3*, 605−618.

(22) Nakatsuji, H. *Chem. Phys.* **1983**, *75*, 425.

(23) (a) Miertus, S.; Scrocco, E.; Tomasi, J. *J. Chem. Phys.* **1981**, *55*, 117. (b) Miertus, S.; Tomasi, J. *J. Chem. Phys.* **1982**, *65*, 239. (c) Cossi, M.; Barone, V.; Cammi, R.; Tomasi, J. *J. Chem. Phys. Lett.* **1996**, *255*, 327. (d) Barone, V.; Cossi, M.; Mennucci, B.; Tomasi, J. *J. Chem. Phys.* **1997**, *107*, 3210.

(24) Dunning, T. H.; Hay, P. J. *Modern Theoretical Chemistry*; Schaefer, H. F., Ed.; Plenum: New York, 1976; Vol. 3, p 1.

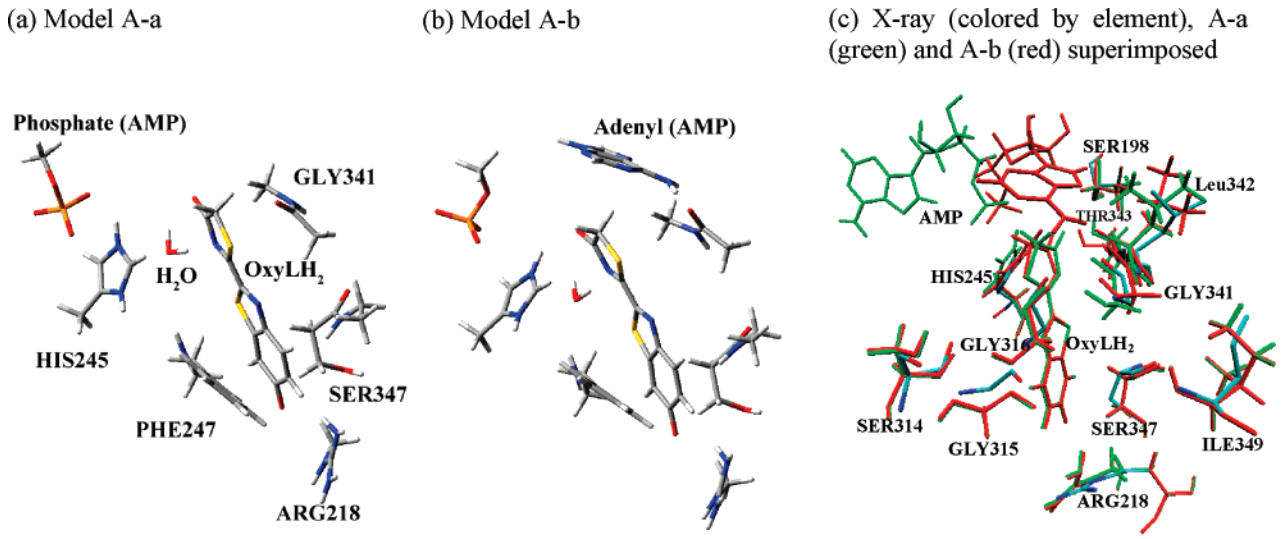

Figure 4. (a, b) Computational models treated by ab initio CIS optimization. Atoms not shown in the figures were treated by the point-charge model. (c) Models A-**a** (green) and A-**b** (red) are compared to X-ray crystallographic structure (colored by elements). Amino acids illustrated have the averaged deviation more than 0.4 Å.

potential curve (GSUM method[25]). The GSUM method guarantees a smooth potential curve despite of the selections of the excitation operators. To ensure the GSUM method accurate, we used the Pipek–Mezey localized molecular orbitals.[26]

Structural Optimization of Luc-$OxyLH_2$ Complex. On the basis of the X-ray structure (1LCI[15]) and the working model proposed in the experimental studies,[10,16] model A and model B (see Figure S1 in the Supporting Information) were constructed as initial guesses, and molecular dynamics (MD) calculations were performed to relax the structures. Both models include hydrogen-bonding with Arg218 as suggested in a previous study.[17] In model A, $OxyLH_2$ is placed in the pocket, so that the carbonyl oxygen in its thiazolinone ring can interact with His245. Model B has the opposite orientation. The results of MD simulations showed that Model A is much more stable than Model B, because of the hydrogen bonding between $OxyLH_2$ and the histidine.

The MD simulations were done with the use of the AMBER94 force-field.[27] The force-field parameters were constructed for the first excited-state of $OxyLH_2$. The equilibrium bond lengths, bond angles, dihedral angles, and electrostatic potential charges were obtained from the geometry optimized by CIS/6-31g*. For the force constants and van der Waals parameters, we used those for a similar "atom type" defined in the AMBER94 force-field.[27] Before the MD simulations, the hydrogen atoms and some missing residues were added to the X-ray (1LCI) structure, and preliminary geometry optimizations were done for these atoms. Classical MD simulations were conducted for $OxyLH_2$, AMP, and selected amino acids and water molecules. If all of the atoms in the amino acids and water molecules were located more than 7.0 Å away from the luciferin, the coordinates were frozen in the simulation. To find the stable structures, the temperature of the MD simulation was raised stepwise up to 300 K. In each step, the temperature was raised by 50 K, and a 10 ps MD calculation was performed to stabilize the structures. At 300 K, a 30 ps MD calculation was made to obtain the reference structure.

After the MD simulation, we extracted two stable structures, A-**a** and A-**b**, from the trajectory obtained with model A. These structures were further refined by the MM and ab initio CIS geometry optimizations. In the CIS calculations, $OxyLH_2$, AMP, ARG218, HIS245, PHE247, GLY341, LEU342, SER347, ALA348, and the crystal water HOH45 were treated with the QM method, and the rest of the protein was treated by the classical point-charge model defined by the MM parameters. The basis sets of 6-31 g* were used for $OxyLH_2$, and the 6-31 g set was used for the rest of the QM atoms. The optimized structures are shown in Figure 4a,b, and their superposition is shown in Figure 4c. These two structures are similar to each other except for the position of the adenyl group. The phosphate group is close to His245, because of the interaction between the negative charge in the phosphate and the positive charge in the His245. Although the gas-phase structure of $OxyLH_2$ is coplanar, the C2–C2′ bond is slightly twisted. For models A-**a**, and A-**b**, the dihedral angles, N=C–C=N, are 170° and 160°, respectively.

Table 1. Averaged Devitation (>0.4 Å) between X-ray (1LCI) and Optimized Structures[a]

	A-**a**	A-**b**	position[b]
Ser198	0.477	0.477	second layer
Arg218	0.431	0.451	first layer
His245	0.471	0.321	first layer
Ser314	0.390	0.403	first layer
Gly315	1.091	1.143	first layer
Gly316	0.728	0.704	first layer
Gly341	0.544	0.454	first layer
Leu342	0.644	0.804	first layer
Thr343	0.212	0.481	first layer
Ser347	0.522	0.490	first layer
Ile349	0.402	0.402	second layer

[a] Deviations in atomic coordinates were averaged within each amino acid. Residues at the protein surface were excluded. [b] See Figure 4c.

We also compared the present optimized structure with the X-ray crystallographic structure of Luc.[15] This structure determination is possible only with the theoretical method because it is for the excited-state of luciferin. Deviations in atomic coordinates between the X-ray and optimized structures were calculated. The amino acids shown in Table 1 and Figure 4c have the averaged deviation more than 0.4 Å. As seen in Table 1 and Figure 4 (c), the residues directly interacting to $OxyLH_2$ show relatively large differences between the X-ray structure (colored by element) and the present optimized geometry (green and black). They rearrange their conformations to enlarge the interaction with $OxyLH_2$. For example, positively charged Arg218 twists its guanidine group toward the carboxy group of $OxyLH_2$. The position of His245 depends to that of AMP. The changes in the main chain of Ser314, Gly315, and Gly316 are due to the insertion of $OxyLH_2$ into the binding site. The insertion also affects Gly341, Leu342, and Thr343.

(25) Nakatsuji, H.; Ushio, J.; Yonezawa, T. *Can. J. Chem.* **1985**, *63*, 1857.
(26) Pipek, J.; Mezey, P. G. *J. Chem. Phys.* **1989**, *90*.
(27) Cornell, W. D.; Cieplak, P.; Bayly, C. I.; Gould, I. R.; Merz, K. M.; Ferguson, D. M.; Spellmeyer, D. C.; Fox, T.; Caldwell, J. W.; Kollman, P. A. *J. Am. Chem. Soc.* **1995**, *117*, 5179.

Table 2. Chemiluminescence (fluorescence) of $OxyLH_2$ Calculated by the SAC−CI Method with D95(d) Basis Sets in the Gas Phase and in Dimethyl Sulfoxide (DMSO) Solution[a]

molecule	environment: optimization	environment: single point	emission energy/eV: SAC–CI	emission energy/eV: exptl
		Keto Forms		
keto-*s*-trans	gas	gas	3.26	1.97[b]
	gas	DMSO	2.95	
keto-*s*-cis(−1)	gas	gas	1.99	
	gas	DMSO	2.08	
keto-*s*-trans(−1)	gas	gas	1.96	
	gas	DMSO	2.08	
	DMSO (with K^+)	DMSO (with K^+)	2.10	
		Enol Forms		
enol-*s*-trans	gas	gas	2.92	2.20[c]
	gas	DMSO	2.83	
enol-*s*-cis(-1)	gas	gas	2.04	
	gas	DMSO	2.30	
enol-*s*-trans(-1)	gas	gas	2.02	
	gas	DMSO	2.25	
	DMSO (with K^+)	DMSO (with K^+)	2.31	
enol-*s*-trans(-1)′	gas	gas		
	gas	DMSO	2.14	
	DMSO (with K^+)	DMSO (with K^+)	2.20	
enol-*s*-trans(-2)	gas	gas	1.85	
	gas	DMSO	2.07	
	DMSO (with $2K^+$)	DMSO (with $2K^+$)	2.17	

[a] The term "with K^+" indicates that the K^+ ion is explicitly included in the QM calculation. [b] Calculation used 0.005 M potassium *tert*-butoxide (K[*tert*-BuO]) in DMSO.[7] [c] Calculation used 0.5 M potassium *tert*-butoxide (K[*tert*-BuO]) in DMSO.[7]

The Cartesian coordinates of the models A-**a** and A-**b** were given in the Supporting Information.

The QM and MM calculations were performed using the Gaussian 03[28] and TINKER[29] programs, respectively.

Results and Discussion

Chemiluminescence: Fluorescence Energies of $OxyLH_2$ in Keto and Enol Forms. The emission energies for the eight isomers calculated by the SAC−CI method are shown in Table 2. All of the isomers have a coplanar structure in the excited state, which agrees with the previous report.[14] The first excited-state is characterized as a one-electron transition from HOMO(π) to LUMO(π^*) in all of the isomers considered in this study.

First, we could exclude the neutral forms, keto-*s*-trans and enol-*s*-trans, from the candidates for the chemiluminescence emitter. The calculated fluorescence energies for keto-*s*-trans and enol-*s*-trans in the DMSO environment are 2.95 and 2.83 eV, respectively. These are much higher than the experimental values obtained for the keto (1.97 eV) and enol (2.20 eV) forms, respectively. Among the trans and cis isomers, we focused on the trans isomers. Although the calculated fluorescence energies for the trans and cis isomers are very close to each other, the total energy of the trans isomer in the excited-state is lower than that of the cis isomer. For instance, in the DMSO environment, the keto-*s*-trans(-1) and enol-*s*-trans(-1) forms are lower than their cis isomers by 6.4 and 5.8 kcal/mol, respectively.

Regarding the keto form, the calculated emission energy for keto-*s*-trans(-1) was 2.10 eV with K^+ ion, which reasonably agrees with the experimental value of 1.97 eV. Thus, keto-*s*-trans(-1) was confirmed as the red emitter in the chemiluminescence.

For the yellow-green emitter under strongly basic conditions, the calculated emission energies of the three candidates, enol-*s*-trans(-1), enol-*s*-trans(-1)′, and enol-*s*-trans(-2), were 2.31, 2.20, and 2.17 eV, respectively. Since all of these values are close to the experimental emission energy of 2.20 eV, we next examined the relative stability of these enol forms in the excited states. The total energy is defined as the sum of those of the potassium-$OxyLH_2$ complex and *tert*-BuO, as shown in Table 3. For instance, the total energy of the enol-*s*-trans(-1) system is the sum of K[enol-*s*-trans(-1)] in the excited-state and K[*tert*-BuO] in the ground state. RHF/6-31g* and CIS/6-31g* plus PCM calculations were carried out for optimizing the structures in the ground and excited states, respectively.

The geometry of *tert*-BuO in the ground state was optimized at RHF/6-31G* plus PCM. As Table 3 shows, enol-*s*-trans(-2) is most stable of the three candidates by 6.7−8.3 kcal/mol. The present calculations thus suggest that enol-*s*-trans(-2) is the most likely candidate for the yellow-green chemiluminescence emitter.

The relative energies shown in Table 3 explain the experimental observation that the keto to enol transformation occurred in the excited-state when an excess of K[*tert*-BuO] was present.[7] The energy of the enol-*s*-trans(-2) system is 10.5 kcal/mol lower than that of the keto-*s*-trans(-1) system. Thus, excess K[*tert*-BuO] can promote the formation of the enol-*s*-trans(-2) form before red-light emission occurs from the keto-*s*-trans(-1) form. In contrast, the energies of the enol-*s*-trans(-1) and enol-*s*-trans(-1)′ systems are 17.2 and 18.8 kcal/mol higher than that of the keto-*s*-trans(-1) system.

We also examined another solvation model in which an explicit DMSO molecule exists between $OxyLH_2$ and K^+. The geometries were optimized at CIS/D95(d) plus PCM(DMSO) level (see structures in Figure S5). The DMSO molecule causes slight red shift in emission energies: 0.03, 0.04, 0.05, and 0.04 eV in keto-*s*-trans(-1), enol-*s*-trans(-1), enol-*s*-trans(-1)′, and enol-*s*-trans(-2), respectively (see CIS emission energies in Table S3).

(28) Frisch, M. J.; et al. *Gaussian 03*, Gaussian, Inc.: Pittsburgh, PA, 2003.
(29) Ponder, J. W.; Ren, P. *J. Phys. Chem. B* **2003**, *107*, 5933.

Table 3. Relative Energy (kcal/mol) for the Excited State of Potassium-$OxyLH_2$ Complex

	computational model[a]	relative energy (kcal/mol)[b]
	(a) tight ion-pair model (without explicit DMSO)[c]	
keto form		
	K[keto-*s*-trans(-1)] + K[*tert*-BuO]	0.0 (10.5)
enol forms		
	K[enol-*s*-trans(-1)] + K[*tert*-BuO]	17.2 (27.7)
	K[enol-*s*-trans(-1)′] + K[*tert*-BuO]	18.8 (29.3)
	K_2[enol-*s*-trans(-2)] + *tert*-BuOH	−10.5 (0.0)
	(b) solvent separated ion-pair model (with explicit DMSO)[c]	
keto form		
	K[DMSO][keto-*s*-trans(-1)] + K[*tert*-BuO] + DMSO	0.0 (6.5)
enol forms		
	K[DMSO][enol-s-trans(-1)] + K[*tert*-BuO] + DMSO	17.6 (24.1)
	K[DMSO][enol-*s*-trans(-1)′] + K[*tert*-BuO] + DMSO	20.1 (26.6)
	K_2[DMSO]$_2$[enol-*s*-trans(-2)] + *tert*-BuOH	−6.5 (0.0)

[a] Computational model for quantum-mechanical calculation. The rest of the solvation effect was treated by the PCM(DMSO). CIS/6-31g* plus PCM calculations were performed for the excited states of the potassium−$OxyLH_2$ complex and potassium−DMSO−$OxyLH_2$ complexes, and RHF/6-31g* plus PCM(DMSO) calculations were performed for the ground state of the *tert*-BuO and DMSO, respectively. [b] Keto-*s*-trans(-1) is taken as the reference. The number in parentheses is the relative energy, with enol-*s*-trans(-2) as the reference. [c] The K^+ ion was directly coordinated by $OxyLH_2$ in "tight ion-pair model", while "solvent separated ion-pair model" includes a DMSO molecule between $OxyLH_2$ and K^+ (see optimized structures in Figure S5).

Bioluminescence: Fluorescence Energy of the Keto-$OxyLH_2$ inside Luc. First, we roughly determined the important residues for the color tuning of the fluorescence. The transition to the first excited state changes the charge distribution of $OxyLH_2$, which affects the interaction energy between $OxyLH_2$ and the surrounding molecules. Figure 5 illustrates the changes in the Mulliken atomic charges of $OxyLH_2$ (keto-*s*-trans(-1) form) upon the excitation, $Q_A^{Ex} - Q_A^G$. In the first excited state, the O4 atom becomes more negative, while the negative charge of the O6′ is decreased upon excitation. The O4 atom is located within 5 Å of His245 (+1 charge) and AMP (−2 charge in the phosphate group), and the O6′ atom has a hydrogen bond with Arg218 (+1 charge). Thus, the difference in the interaction energy between the ground and excited states (ΔE) would contribute to the shift in the emission energy caused by the Luc environment.

$$\Delta E = \sum_{M}^{\text{residues}} \Delta E_M = \sum_{M}^{\text{residues}} \{E_M^{Ex} - E_M^G\} = \sum_{M}^{\text{residues}} \left\{ \sum_{A}^{OxyLH_2} \sum_{B\in M}^{\text{others}} \frac{Q_A^{Ex} Q_B}{r_{AB}} - \sum_{A}^{OxyLH_2} \sum_{B\in M}^{\text{others}} \frac{Q_A^{G} Q_B}{r_{AB}} \right\} \quad (1)$$

ΔE can be easily decomposed into the contributions from each protein residue $\Delta E_M (= E_M^{Ex} - E_M^G)$, where E_M^{Ex} and E_M^G are the interaction energies in the excited and ground states, respectively. We evaluated the interaction energy as the classical Coulombic atomic charge interaction between $OxyLH_2$ and the surrounding molecules. The atomic charges of $OxyLH_2$ in the ground Q_A^G and the excited Q_A^{Ex} state were obtained by electrostatic potential fitting[30] using HF and CIS wave functions, respectively. Those of the residues Q_B were taken from the AMBER94 force-field. The result of the decomposition analysis is shown in Figure 6. The positive and negative contributions indicate spectral blue- and red-shifts in the fluorescence, respectively. It is clear that Arg218, His245, and AMP (phosphate group) give dominant contributions. Arg218 and AMP cause the blue-shifts of 0.29 and 0.21 eV, respectively, and His245 contributes to the red-shift of 0.17 eV. Overall, net ΔE becomes positive, and the surrounding residues and AMP lead to the blue-shift in the emission energy. However, since these contributions seem to be too large to be treated by the

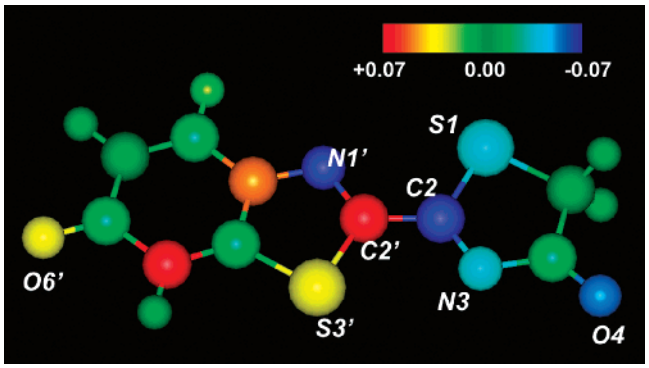

Figure 5. Difference in Mulliken atomic charge between the ground and the first excited state of $OxyLH_2$ (keto-*s*-trans form), $Q_A^{Ex} - Q_A^G$. The color of the atoms shows the change in the atomic charges.

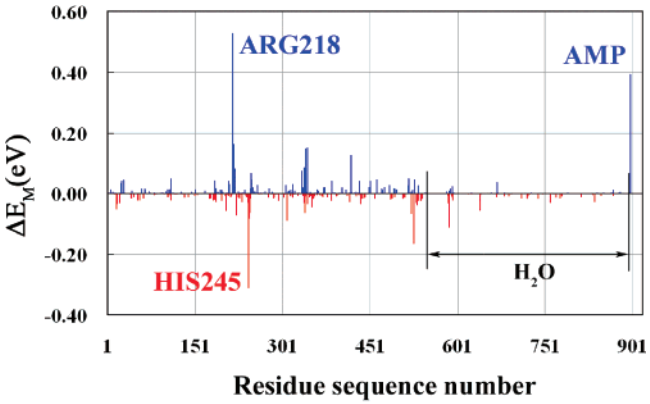

Figure 6. Decomposition analysis of ΔE ($= E^{Ex} - E^G$, difference in interaction energy between the ground and the excited state). ΔE was decomposed into contributions from the protein residues and from AMP, ΔE_M. Positive and negative contributions indicate spectral blue- and red-shifts in fluorescence, respectively.

(30) Besler, B. H.; Merz, K. M., Jr.; Kollman, P. A. *J. Comp. Chem.* **1990**, *11*, 431.

Table 4. Emission (Fluorescence) Energies of $OxyLH_2$ in the Keto-*s*-trans(-1) Form in the Gas Phase and Protein Environment

				emission energy/eV	
calcn	environment	QM region	geometry[a]	SAC-CI	exptl
1	in gas phase	$OxyLH_2$	gas	1.97	
2		$OxyLH_2$	A-**a**	1.73	
			A-**b**	1.58	
3	in protein	$OxyLH_2$	A-**a**	2.02	
			A-**b**	1.82	
4		+ ARG218	A-**a**	2.07	
			A-**b**	1.90	
5		+ HIS245	A-**a**	2.22	
			A-**b**	2.01	
6		+ phosphate	A-**a**	2.33	2.23[b]
			A-**b**	2.08	
7		+PHE247, GLY341, EU342, SER347, LA348, HOH45	A-**a**	(2.24)[c]	2.23[b]
			A-**b**	(1.95)[c]	

[a] "gas" denotes geometry optimized in the gas phase. For structures "A-**a**" and "A-**b**", see computational details. [b] Bioluminescence emission maxima for *Photinus pyralis* wild-type at pH 8.6.[9] [c] Energy correction due to the QM effect from the additional residues was estimated with eq 2 (see text).

electrostatic interactions alone, we treated Arg218, His245, and the phosphate group of AMP by the QM calculations with the SAC−CI method.

Table 4 shows the fluorescence energy calculated by the SAC−CI method using various computational models. The best calculation includes Arg218, His245, and the phosphate group, and is referred to as calcn 6. Models A-**a** and A-**b** in calcn 6 gave the excitation energies of 2.33 and 2.08 eV, respectively, as shown in Table 4. These values are close to the experimental emission energy (2.23 eV). The excitation is essentially one-electron transition from HOMO to LUMO, and these orbitals are clearly localized within $OxyLH_2$, as shown in Figure 7a. This result suggests that the keto-form of $OxyLH_2$ can produce yellow-green luminescence. It agrees with the experiment by Branchini et al.,[9] which showed that yellow-green emission was produced even by a keto-constrained $OxyLH_2$ analogue. It is not necessary to assume keto−enol tautomerism to explain the blue-shift of the emission wavelength. We also considered the possibility of the enol forms (see subsection of "microenvironmental mechanism").

Next, the origin of the blue-shift was analyzed by comparing several SAC−CI calculations using different computational models. Table 5 summarizes the methods of the analyses and the results. The reference gas-phase SAC−CI calculation (calcn 1) gives an excitation energy of 1.97 eV. This calculation used the optimized geometry in the gas phase, and no environmental effect was included. In calcn 2, all of the surrounding molecules were removed from the computational models used in calcn 6. Comparison between calcn 2 and calcn 1 gives the chromophore structural effect on fluorescence energy. The excitation energies obtained were 1.73 and 1.58 eV for models A-**a** and A-**b**, respectively. The structural constraint in the protein environment caused red-shifts in the fluorescence by 0.24 and 0.39 eV, respectively. This is because $OxyLH_2$ loses its coplanarity in the protein environment. Figure 8 shows the potential energy curves along the rotation of the C2−C2′ bond of $OxyLH_2$ (keto-*s*-trans(-1) form) in the gas phase. Since the energy of the ground state becomes more unstable than that of the first excited state, the C2−C2′ rotation reduces the emission energy.

Comparison between calcn 2 and calcn 6 corresponds to the environmental effect on the emission energy caused by the Coulombic interaction between $OxyLH_2$ and the surroundings.

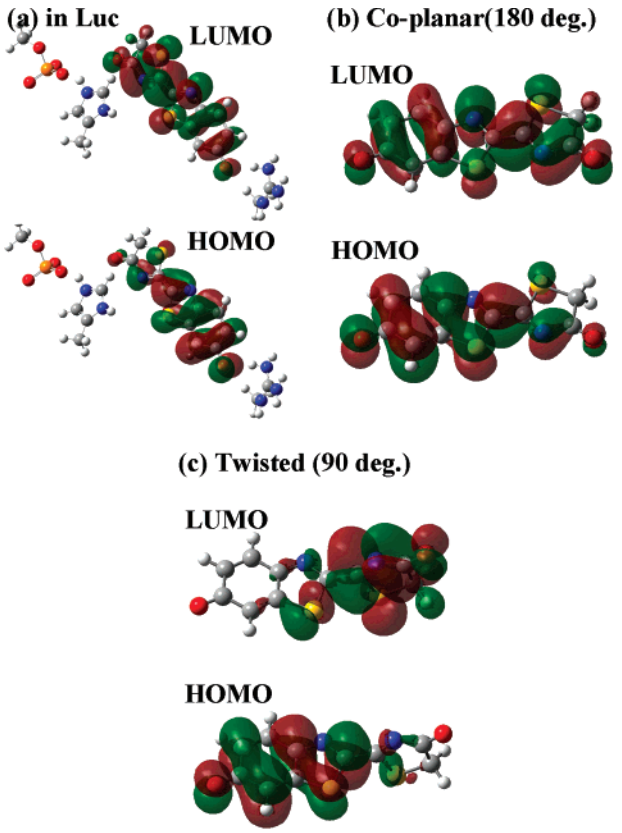

Figure 7. Highest-occupied canonical molecular orbital (HOMO) and lowest-unoccupied canonical molecular orbital (LUMO) of $OxyLH_2$ in (a,b) coplanar and (c) twisted structures. Red, blue, yellow, gray, and white balls denote O, N, S, C, and H atoms, respectively.

This environmental effect leads to a marked blue-shift in fluorescence energy of 0.60 and 0.50 eV in models A-**a** and A-**b**, respectively. To understand the origin of the shift, we performed further analyses using several SAC−CI results. In calcn 3, all of the surroundings were treated by the point-charge model. The calculated emission energies were 2.02 and 1.82 eV for models A-**a** and A-**b**, respectively. Classical interaction contributes to the blue-shift, but the amounts of the shifts (0.29 and 0.24 eV for A-**a** and A-**b**, respectively) are smaller than those obtained with calcn 6. This indicates that the classical

Table 5. Protein Effect on Emission Energy Analyzed by the SAC−CI Calculations Given in Table 4. See Text for Detailed Explanations

effect on the emission energy estimated by the series of SAC−CI calculations		geometry[a]	shift in emission energy (eV)
total protein effect	Δ(calcn 6 − calcn 1)	A-**a**	+0.36 (+0.27)[f]
		A-**b**	+0.11 (−0.02)[f]
structure of $OxyLH_2$	Δ(calcn 2 − calcn 1)	A-**a**	−0.24
		A-**b**	−0.39
total environmental effect	Δ(calcn 6 − calcn 2)	A-**a**	+0.60 (+0.51)[f]
		A-**b**	+0.50 (+0.37)[f]
classical Coulombic effect[b]	Δ(calcn 3 − calcn 2)	A-**a**	+0.29
		A-**b**	+0.24
quantum mechanical effect[c]	Δ(calcn 6 − calcn 3)	A-**a**	+0.31 (+0.22)[f]
		A-**b**	+0.26 (+0.13)[f]
Only ARG218 in QM region[d]	Δ(calcn 4 − calcn 3)	A-**a**	+0.05
		A-**b**	+0.08
ARG218 and HIS245 in QM region[e]	Δ(calcn 5 − calcn 3)	A-**a**	+0.20
		A-**b**	+0.19

[a] "A-**a**" and "A-**b**" denote the structures A-**a** and A-**b**, respectively (see computational details). [b] All of the residues and AMP were treated by the point-charge model. [c] Arg218, His245, and the phosphate group of AMP were treated by the QM method. The rest were treated by the point-charge model. [d] Only Arg218 was included in the QM region in the SAC−CI calculation. The rest of the residues and AMP were treated by the point-charge model. [e] Arg218 and His245 were included in the QM region in the SAC−CI calculation. The rest of the residues and AMP were treated by the point-charge model. [f] The number in parentheses was obtained using calcn 7 instead of calcn 6 in Table 4. The QM effects from some other residues were evaluated at CIS level.

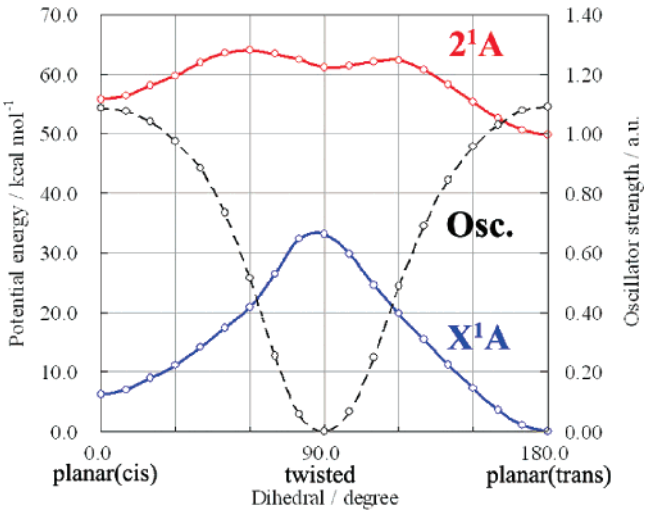

Figure 8. Potential energy curves along the rotation of the C2−C2′ bond of $OxyLH_2$ (keto-*s*-trans(-1) form) in the gas phase. The other geometrical parameters were optimized at each point by CIS calculations for the first excited state. Oscillator strength in au (dashed line) is also shown.

treatment cannot sufficiently describe the interactions between $OxyLH_2$ and the surroundings.

Next, Arg218 was included in the QM region (calcn 4). The calculated emission energies increased slightly to 2.07 and 1.90 eV for models A-**a** and A-**b**, respectively. We also included His245 in the QM region. The calculated emission energies became 2.22 and 2.01 eV, respectively. Inclusion of the phosphate group increased the excitation energies to 2.33 and 2.13 eV, respectively. The QM effect of Arg218, His245, and the phosphate group was estimated to be 0.05/0.08, 0.15/0.11, and 0.11/0.12 eV for model A-**a**/A-**b**, respectively. Thus, the QM effect from these residues also produces a spectral blue-shift of the fluorescence energy.

To investigate the QM effect of other neighboring residues and water molecules, we additionally included Phe247, Gly341, Leu342, Ser347, Ala348, HOH45 into the QM model (see Figure 4a,b for the computational model). Since SAC−CI calculation of such a large QM model is practically difficult at present, we applied an ONIOM-like estimation[31] at the CIS/D95(d) level.

$$\mathrm{EE(large, SAC{-}CI + CIS)} = \{\mathrm{EE(large, CIS)} - \mathrm{EE(small, CIS)}\} + \mathrm{EE(small, SAC{-}CI)} \quad (2)$$

The correction obtained by this scheme was −0.09 and −0.13 eV for model A-**a** and model A-**b**, respectively. The estimated emission energies became 2.24 and 1.95 eV, respectively. Even though this correction is taken into account, the analysis in Table 5 shows that the total environmental effect gives a marked blue-shift in the emission energy: +0.51 and +0.37 eV for model A-**a** and model A-**b**, respectively.

On the Possibility of the TICT State Mechanism: Potential-Energy Surface of the First Excited State of $OxyLH_2$. We now discuss the possibility of the TICT state as the emitting state. Figure 8 shows the gas-phase potential-energy curves for the C2−C2′ rotation (Figure 1c) calculated at the SAC−CI/D95(d)//CIS/D95(d) level. The calculated oscillator strength (emission intensity) is also shown.

The character of the first excited state is HOMO−LUMO transition. In the coplanar structure, both HOMO and LUMO are delocalized over the entire molecule, as shown in Figure 7b. In the twisted structure, however, the HOMO and LUMO are clearly localized on the benzothiazolyl ring and the thiazolinone ring, as shown in Figure 7c. These orbitals are very similar to the HOMO and LUMO of benzothiazole and thiazole, respectively. Since the first excited state in the twisted structure is a one-electron transition from HOMO to LUMO, the nature of the state is a charge-transfer state. The ground-state electronic structure is dominated by the closed-shell determinant. The coefficient of the double excitation operators is less than 0.1 in the SAC wave function.

On the potential surface of the first excited state, there are three stationary points: coplanar structures (0° and 180°) and a twisted structure (91°), both at the SAC−CI and CIS levels. The twisted structure is less stable than the coplanar structures. The energy barriers toward the coplanar structures are very small (less than 4 kcal/mol) in the first excited state. In contrast, the energy barriers to the twisted structure are 12.6 and 8.3 kcal/mol from the trans and the cis side, respectively. In addition, the oscillator strength for the fluorescence from the first excited-state becomes close to zero in the twisted structure but is very large in the coplanar structures, as shown in Figure 8.

Based on our present results, even if $OxyLH_2$ became the TICT excited-state during the photochemical processes, it could relax to a coplanar structure owing to the small energy barrier. In addition, the fluorescence intensity is low in the twisted charge-transfer state. Therefore, the emitting state of $OxyLH_2$ should be a coplanar structure, and the TICT state mechanism is unrealistic.

On the Microenvironmental Mechanism. The hydrogen bonds between $OxyLH_2$ and the local environment have been implicated in the mechanism of the color tuning in the firefly luminescence.[13,14] In this section, we discuss how this mechanism is relevant to yellow-green emission.

(31) Maseras, F.; Morokuma, K. *J. Comp. Chem.* **1995**, *16*, 1170.

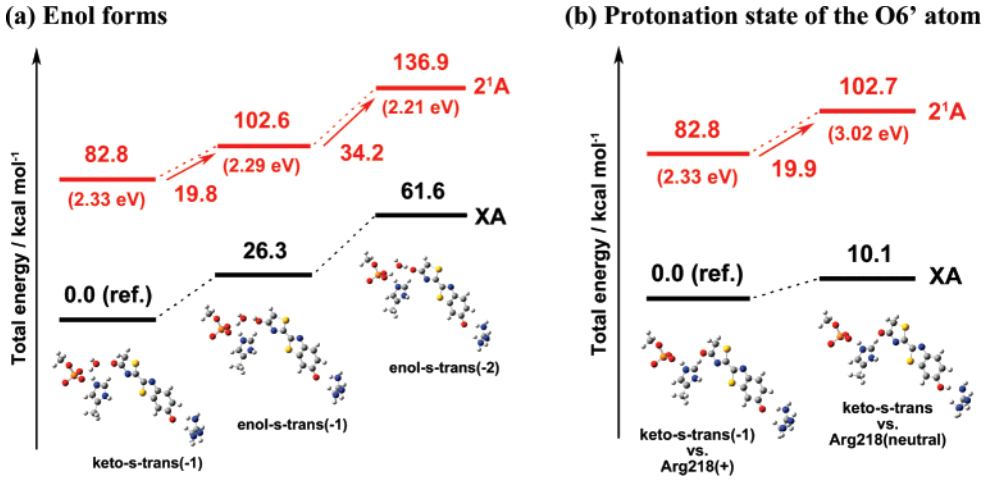

Figure 9. (a) Comparison of the potential energy and emission energy (in parenthesis) of the keto and enol forms in the Luc environment; (b) comparison of the potential energy and emission energy (in parentheses) of the two protonation states.

First, the possibility of the enol form[13,14] was considered. Although Branchini and co-workers showed that keto-constrained $OxyLH_2$ emits yellow-green luminescence,[9,10] an enol transformation due to the local environment cannot be excluded in the case of the actual keto-$OxyLH_2$. We performed the SAC−CI calculations with CIS/6-31G* optimized geometry for enol-*s*-trans(-1) and enol-*s*-trans(-2) inside Luc. In both the enol-*s*-trans(-1) and the enol-*s*-trans(-2) structures, a crystal water molecule (HOH128) was located between the enol-$OxyLH_2$ and the phosphate group. In the enol-*s*-trans(-2) structure, the enol form was deprotonated, and the proton was transferred to the phosphate group. The fluorescence energy and energy profile are shown in Figure 9a, together with the optimized structures. The SAC−CI fluorescence energies (data in the parentheses) of keto-*s*-trans(-1), enol-*s*-trans(-1), and enol-*s*-trans(-2) in Luc were 2.33, 2.29, and 2.21 eV, respectively. All of them are close to the experimental value (2.23 eV). However, the total energy of the first excited-state of the enol-*s*-trans(-1) and enol-*s*-trans(-2) structures are 19.8 and 34.2 kcal/mol higher than that of the keto-*s*-trans(-1) structure, respectively. Although the present CIS calculations are not quantitative, these energy differences are large enough for us to conclude that the enol transformation is energetically unfavorable in the Luc environment.

We now discuss the protonation state of the O6′ atom[13,14] in the benzothiazoryl ring of $OxyLH_2$. We examined another protonation state in which Arg218 is neutral and the proton is transferred to $OxyLH_2$ (Figure 1d). The SAC−CI/D95(d) calculation was performed at the CIS/6-31G* optimized geometry. As shown in Figure 9b, the calculated fluorescence energy was 3.02 eV, which is about 0.8 eV higher than the experimental value. In addition, the total energy evaluated at the CIS/6-31g* level was 20.2 kcal/mol higher than that of the keto-*s*-trans(-1) system. Therefore, we conclude that the neutral keto-$OxyLH_2$ (ketos-*s*-trans form) is not the emitting state in bioluminescence.

On the Resonance-Based Mechanism. The mechanism originally reported was on the resonance structure in the excited state.[10] Here, we discuss how the resonance structures in both the ground and excited states affect the emission energy of keto-$OxyLH_2$. Since resonance structures are components of a wave function, the resonance structures characterize the properties of the state (including geometry). The optimized bond lengths of

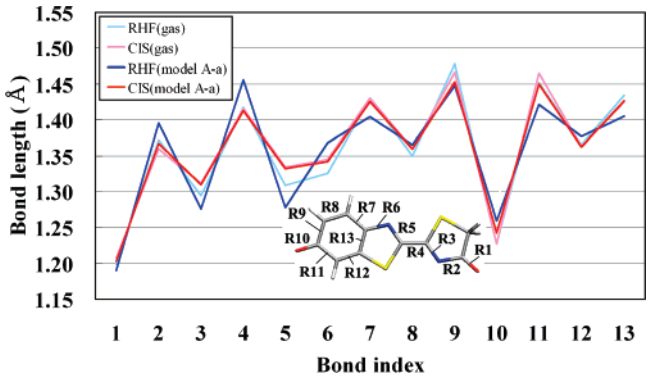

Figure 10. Bond lengths of the ground and the first excited state of keto-$OxyLH_2$ in the Luc environment (A-**a**) and in the gas phase optimized by HF and CIS methods.

$OxyLH_2$ (keto-*s*-trans(-1)) are compared in Figure 10. The calculations were performed at RHF/6-31g* and CIS/6-31g* levels for the ground and the excited state, respectively. The bond lengths for the first excited-state in Luc are very close to those in the gas phase (the rms deviation is 0.007 Å). This clearly indicates that the Luc environment leads to only small changes in the resonance structure in the excited state. In this sense, the original concept of the resonance structure-based mechanism differs from the actual mechanism of yellow-green luminescence.

In contrast, the bond length of the ground state is influenced by the Luc environment. The rms deviation in bond length between the gas phase and Luc is 0.028 Å, and the maximum deviation amounts to 0.05 Å at R3, R4, and R5 (see Figure 10 for a definition of the bond labels). The bond-length alternation becomes marked in the Luc environment, indicating that the resonance structure in the ground state is more like the keto structure (left in Figure 1e). The ground-state relaxation energy from the excited-state geometry to the ground-state one is estimated to be 0.20 eV in Luc and 0.05 eV in the gas phase at the RHF/6-31g* level of calculation. However, such a structural change in the ground state enlarges the Stokes shift. To explain the blue shift in the emission energy, other blue-shift contributions (the protein electrostatic effect) should be larger than the red-shift effect of Stokes shift. Therefore, the structural change between the ground and excited states cannot explain the blue-shift in the Luc environment.

Conclusions

The yellow-green luminescence from firefly Luc of the North American firefly (*P. pyralis*) has long been ascribed to the enol form of $OxyLH_2$.[7] Recently, however, Branchini et al. showed that 5,5-dimethylluciferin constrained to the keto form can produce yellow-green emission in Luc.[10] In the present study, we theoretically determined the structure of the Luc-$OxyLH_2$ complex in the excited state: this is possible only with the theoretical method, since it is the geometry in the excited state. The SAC−CI calculations were performed to calculate the fluorescence energies at the obtained structures.

The present SAC−CI results consistently explained the colors of firefly fluorescence produced by both chemiluminescence and bioluminescence. Depending on the environment, the emission energy shows a marked shift. The keto form of $OxyLH_2$ produced red-light chemiluminescence in solution (1.97 eV in experimental and 2.10 eV in SAC−CI theory). However, in the environment of Luc, the interaction with the nearby protein residues and AMP and the protein electrostatic effect causes the emission energy of the keto form to shift markedly to a higher-energy region corresponding to green light (2.23 eV experimental and 2.08−2.33 eV in SAC−CI theory). The detailed analysis indicates that Arg218, His245, and the phosphate group of AMP play important roles in the color-tuning mechanism, together with the protein electrostatic effect in the Luc environment.

Alternative mechanisms proposed in the previous studies were also examined but were not supported: (1) The TICT state[11] is meta stable on the potential surface. However, it can easily relax to a coplanar structure owing to the small activation barriers (around 2−4 kcal/mol). (2) The emission energy of enol-$OxyLH_2$ is very close to that of the keto form. However, the keto−enol transformation is difficult, since the enol forms are energetically unstable in Luc environment. (3) The protonation state of the O6′ atom significantly affects the emission energy, as described previously.[14] However, proton transfer from Arg218 to keto-$OxyLH_2$ is energetically unfavorable. In addition, the emission energy is far above the observed value. (4) The resonance structures of $OxyLH_2$[10] in the ground and the excited state were also investigated. The resonance structure in the excited state would not be sensitive to the local environment.

The present theoretical analysis could determine the origin of the emission color tuning at amino acid level. On the basis of the result, it is straightforward to perform a theoretical mutation to simulate the emission energies of the mutants, which is an ongoing project in our group.

Last, we note that to study the color-tuning mechanism in chemiluminescence and bioluminescence, the theory used must be reliable enough for reproducing the excitation and luminescent energies. Otherwise, we can never do reliable analysis. In this sense, the SAC−CI method was very useful in the present study. For analyzing the principles and mechanisms behind the complex phenomena, the theory and the method used as a tool must be reliable enough, otherwise it may lead to erroneous conclusion.

Acknowledgment. The authors thank Prof. S. Hayashi (Kyoto University) for the discussion. This study was supported by a Grant-in-Aid for Creative Scientific Research and for Young Researchers from the Ministry of Education, Culture, Sports, Sciences, and Technology of Japan. A part of the computations was performed in the Research Center for Computational Science, Okazaki, Japan and in Kyoto University Data Processing Center. This study was also supported by a Grant-in-Aid for Young Scientists from Computing Service Group, ACCMS and IIMC, Kyoto University.

Supporting Information Available: Complete ref 28; structure of the preliminary computational models, model A and model B; comparison of the fluorescence energy obtained with the CIS and SAC−CI geometries; explanation about the SAC−CI applications; choice of the basis sets for geometry optimization and SAC−CI calculation; CIS structures and emission energies in DMSO solution calculated at CIS/D95(d) level; Cartesian coordinate of model A-**a** and model A-**b** optimized using CIS method. This material is available free of charge via the Internet at http://pubs.acs.org.

JA0611691